ARTICLES
https://doi.org/10.1038/s41557-020-0530-4

nature chemistry

Using sulfuramidimidoyl fluorides that undergo sulfur(VI) fluoride exchange for inverse drug discovery

Gabriel J. Brighty[1,2,10], Rachel C. Botham[1,2,6,10], Suhua Li[1,7,10], Luke Nelson[1], David E. Mortenson[1,2,8], Gencheng Li[1], Christophe Morisseau[3,4], Hua Wang[1,9], Bruce D. Hammock[3,4], K. Barry Sharpless[1,5] ✉ and Jeffery W. Kelly[1,2,5] ✉

Drug candidates that form covalent linkages with their target proteins have been underexplored compared with the conventional counterparts that modulate biological function by reversibly binding to proteins, in part due to concerns about off-target reactivity. However, toxicity linked to off-target reactivity can be minimized by using latent electrophiles that only become activated towards covalent bond formation on binding a specific protein. Here we study sulfuramidimidoyl fluorides, a class of weak electrophiles that undergo sulfur(VI) fluoride exchange chemistry. We show that equilibrium binding of a sulfuramidimidoyl fluoride to a protein can allow nucleophilic attack by a specific amino acid side chain, which leads to conjugate formation. We incubated small molecules, each bearing a sulfuramidimidoyl fluoride electrophile, with human cell lysate, and the protein conjugates formed were identified by affinity chromatography–mass spectrometry. This inverse drug discovery approach identified a compound that covalently binds to and irreversibly inhibits the activity of poly(ADP-ribose) polymerase 1, an important anticancer target in living cells.

In conventional drug discovery approaches, a large number of small molecules are screened for their ability to modify the function of an isolated target protein or a particular cellular phenotype[1]. These approaches can yield hits that exert their action by both covalent and non-covalent mechanisms. Drugs that form covalent conjugates with their targets have historically been avoided due to off-target toxicity concerns, but they can offer potential benefits over non-covalent inhibitors in terms of increased duration of action, lower dosing requirements and the possibility of decreased development of resistance[2,3]. Therefore, we have developed an inverse drug discovery (IDD) strategy, which involves individually reacting a small collection of diverse organic compounds that harbour a weak, but activatable, electrophile with the human proteome in cell lysate to identify the protein(s) targeted[4]. This method identifies numerous nucleophilic sites within the human proteome using only a handful of mildly reactive compounds.

An earlier IDD study using arylfluorosulfates activated towards covalent bond formation by the geometry and composition of the complementary protein binding sites afforded both enzyme and non-enzyme conjugates[4]. From this study, we learned that the presence of a suitable protein binding pocket allows the electrophilic sulfur centre to be placed proximal to a tyrosine or lysine side-chain nucleophile, which enables the sulfur(VI) fluoride exchange (SuFEx) reaction to proceed[4–6]. The additional presence of a nearby cationic arginine and/or lysine side chain seems to be critical to lower the barrier for the SuFEx reaction, as these residues probably facilitate extraction of the fluoride ion. These cationic residues may also perturb the reactive side chain's pK_a, and so enhance its nucleophilicity[4]. The potential of SuFEx reactions employing sulfonyl fluorides and arylfluorosulfates has been demonstrated in the fields of material science[7–9] and late-stage drug functionalization to enhance the pharmacologic activity[10].

Here we apply the IDD approach[4,6] to another family of SuFEx-derived electrophiles, the sulfuramidimidoyl fluorides (SAFs)[11], whose proteome reactivity has not been previously assessed. We explored the hypothesis that the unique chemical environments within proteins should allow the use of less-reactive SuFEx-derived SAFs for IDD. The SAFs were prepared by a two-step SuFEx reaction process (Fig. 1a)[11]. First, an alkyl or aryl primary amine was reacted with thionyl tetrafluoride (SOF_4) at a standard temperature and pressure in the presence of two equivalents of an organic base to produce the corresponding iminosulfur oxydifluoride. Next, a secondary amine was used to displace one of the remaining fluorides in the presence of triethylamine to produce the corresponding SAF (Fig. 1a). The reduced electrophilicity of the SAFs compared with arylfluorosulfates in acetonitrile probably arises from the replacement of a S=O bond with a S=NR bond, which increases the electron density around the sulfur centre in SAFs to afford an even stronger bond between the fluorine and sulfur[11]. Although the sulfur centres in both SAFs and arylfluorosulfates are tetrahedral, in SAFs this centre is also chiral[11].

In this study, we matched SAFs with the human protein(s) that they react with using affinity chromatography–mass spectrometry. Selected conjugation reactions were then validated using

[1]Department of Chemistry, The Scripps Research Institute, La Jolla, CA, USA. [2]Department of Molecular Medicine, The Scripps Research Institute, La Jolla, CA, USA. [3]Department of Entomology and Nematology, University of California Davis, Davis, CA, USA. [4]UC Davis Comprehensive Cancer Center, University of California Davis, Davis, CA, USA. [5]The Skaggs Institute for Chemical Biology, The Scripps Research Institute, La Jolla, CA, USA. [6]Present address: Codexis, Redwood City, CA, USA. [7]Present address: School of Chemistry, Sun Yat-Sen University, Guangzhou, P. R. China. [8]Present address: Gilead Sciences Inc., Foster City, CA, USA. [9]Present address: Sorrento Therapeutics, Inc., San Diego, CA, USA. [10]These authors contributed equally: Gabriel J. Brighty, Rachel C. Botham, Suhua Li. ✉e-mail: sharples@scripps.edu; jkelly@scripps.edu

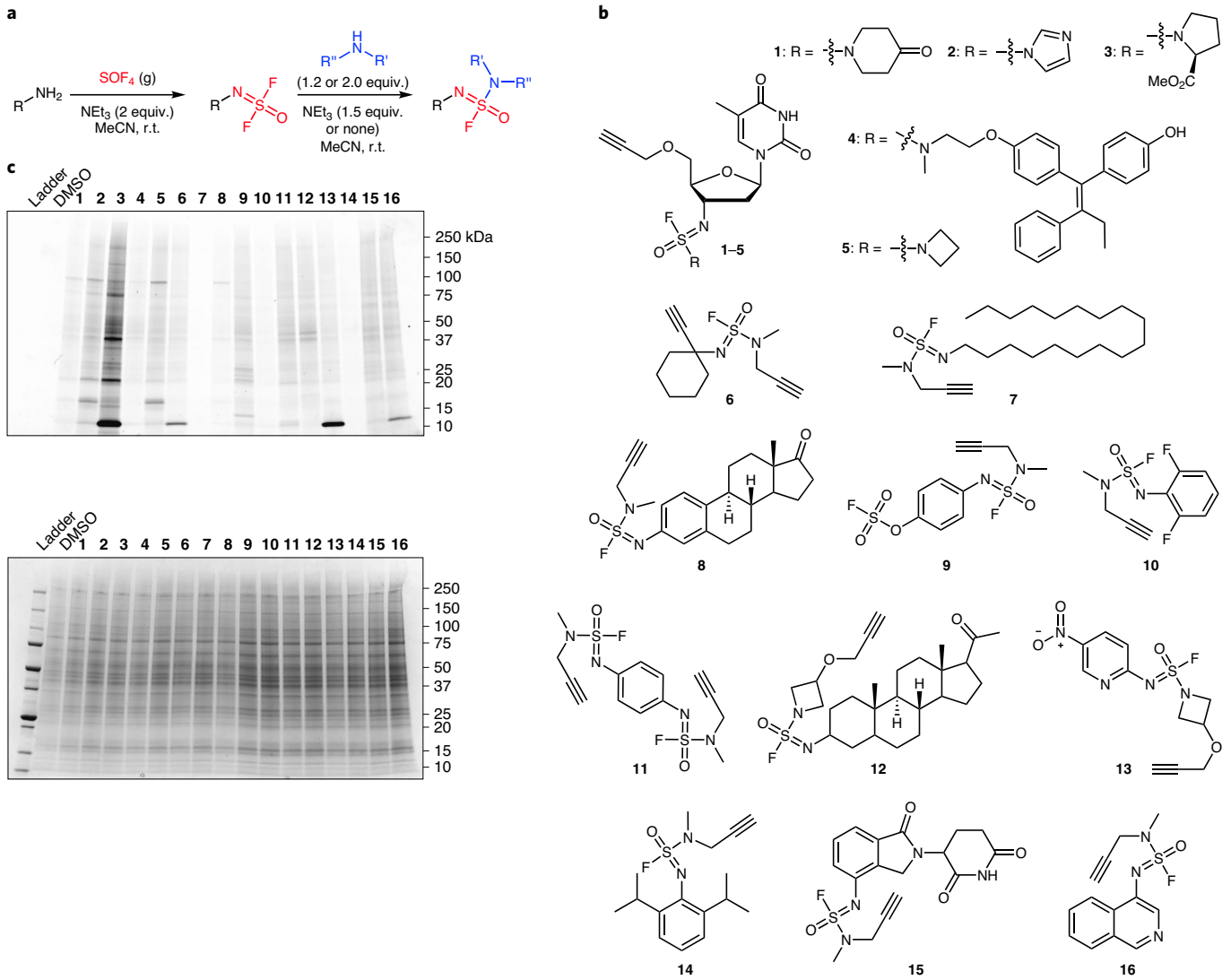

Fig. 1 | SAFs 1–16 react with proteins in HEK293T cell lysate. a, Stepwise synthetic scheme for the synthesis of SAF-containing compounds. A primary amine was reacted with SOF_4 to form an iminosulfur oxydifluoride. This intermediate was then reacted with a secondary amine to form as SAF. **b**, Structures of SAF compounds **1**–**16** used in this study. **c**, Top: SDS-PAGE/rhodamine analysis of HEK293T lysate incubated (18 h) with the SAF compound (50 μM), after the addition of TMR-N_3 via CuAAC (see Methods for detailed conditions). Each SAF appears to react with a different set of proteins, as indicated by the different banding patterns in each lane. Bottom: Coomassie staining of the SDS-PAGE gel indicates an equal loading of protein in each lane. The fluorescence intensity of each band is a product of SAF reactivity towards that protein rather than a difference in protein abundance between treated HEK293T lysates. This experiment was conducted twice ($n = 2$) with similar results. r.t., room temperature.

recombinant proteins in vitro. We demonstrate that structurally distinct SAFs react with different sets of human proteins. Lastly, we matched a thymidine-based SAF with poly(ADP-ribose) polymerase 1 (PARP1), and demonstrated covalent inhibition of PARP1 both in vitro and in live cells, potentially complementing the non-covalent PARP1 inhibitors used to ameliorate cancer.

Results

SAFs react with human proteins. We set out to survey the human proteome for its reactivity with 16 SAF-containing compounds (Fig. 1b). Compounds **1**–**16** comprise largely unpublished SAFs harbouring terminal acetylenes available at the outset of this study[11]. We purposefully did not try to select for motifs that would bind to a particular protein family, although we did use our intuition to maximize the structural diversity. Each SAF was individually incubated with HEK293T cell lysate for 18 hours. The extent of reaction between a given SAF and the targeted proteins increased linearly over 24 hours (Supplementary Fig. 1). Therefore, we chose an incubation period of 18 hours as a practical experimental time point to capture sufficient quantities of SAF-conjugated proteins. The 16 conjugation reactions were then subjected to a copper(I)-catalysed azide–alkyne cycloaddition (CuAAC) reaction[12,13] with tetramethylrhodamine azide (TMR-N_3) and the conjugates were separated in a denaturing gel (SDS–polyacrylamide gel electrophoresis (SDS–PAGE)) visualized by tetramethylrhodamine fluorescence (Fig. 1c). Notably, compounds **1**–**16** displayed different reactivity profiles towards the human proteome detectable by SDS–PAGE, which indicates that the equilibrium binding fragments of these compounds are critical determinants of selectivity for the conjugation process. To more comprehensively survey the conjugates formed and to detect lower-abundance conjugates, we utilized quantitative liquid chromatography–tandem mass spectrometry (LC–MS/MS)[4].

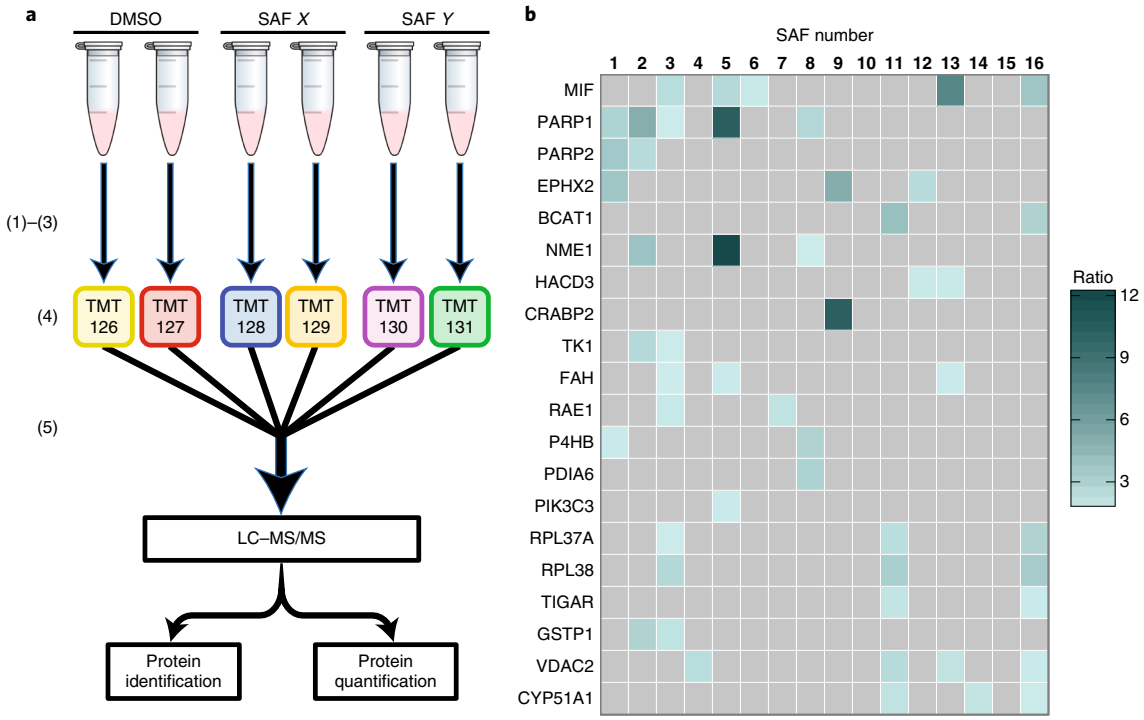

Fig. 2 | Proteins targeted by SAFs 1–16 identified using isobaric MS/MS tagging in conjunction with proteomic mass spectrometry. a, TMT LC–MS/MS workflow. After the HEK293T lysates were treated with a particular probe (50 μM) for 18 h, (1) they were (subject to a CuAAC reaction with biotin-N_3. Next, (2) the protein–probe conjugates were enriched using streptavidin resin and the bound proteins were eluted from the resin using $Na_2S_2O_4$. (3) The enriched conjugates were then digested with trypsin and (4) the resulting peptides were labelled with the respective TMT reagent. (5) The tagged peptides were pooled and subjected to LC–MS/MS based on multidimensional protein identification technology, which allows for protein identification and quantification compared with DMSO controls. **b**, Heat map displaying enrichment ratios of probes **1–16** for selected proteins by quantitative LC–MS/MS. The displayed proteins have enrichment ratios >1.50 (treated samples versus DMSO control), and *P* values <0.25 (calculated by a two-tailed, unpaired *t*-test). Grey squares indicate a failure to make this cutoff. Data are the result of a single experiment that contained two replicate treatment conditions ($n = 2$). See Supplementary Information for the precise enrichment ratios and exact *P* values.

Proteomics identifies the targets of SAFs 1–16. To identify the human proteins targeted by SAFs **1–16**, we subjected the 16 proteome-labelling reactions (18 hours of incubation at 25 °C) to CuAAC reactions with a reductively cleavable biotin azide (biotin-N_3) (refs. [12–14]). The SAF-conjugated proteins were subsequently enriched via streptavidin affinity chromatography. Sodium dithionite ($Na_2S_2O_4$) was used to elute the bound proteins from the streptavidin resin. Enriched proteins were then digested with trypsin and subjected to tandem-mass tag (TMT) labelling[15] to enable the quantification of the SAF–protein conjugates relative to a proteome cell lysate sample treated with dimethylsulfoxide (DMSO) (as the vehicle, but otherwise identically treated) by LC–MS/MS (Fig. 2a). We defined the enrichment ratio for each protein as the 'average of the TMT reporter ion intensity for a given protein in the SAF-treated samples'/'average of the TMT reporter ion intensity for that same protein in the vehicle-treated samples'. Proteins were ranked according to this enrichment ratio. Duplicate measurements of each treatment condition (SAF treated versus DMSO treated) were compared by their enrichment ratios and statistical significance to assess the reliability of each protein target identification. We prioritized protein 'hits' that exhibited a strong enrichment relative to that of the vehicle treated (enrichment ratios >1.5) and a reasonable statistical agreement between duplicate measurements (*P* values <0.25). Additionally, we noted the strong enrichment of several proteins with different SAFs, which further indicates that these proteins are reactive towards SAFs.

As observed in the SDS–PAGE-based comparisons (Fig. 1c), LC–MS/MS analysis of SAFs **1–16** reacting with human cell lysate (HEK293T) revealed substantial differences in the set of protein conjugates formed from distinct SAFs (Fig. 2b depicts a sampling of SAF-reactive proteins). The SAFs appear to target proteins with a variety of functions, which include both enzymes and non-enzymes (Supplementary Fig. 2a,b). Structural proteins and proteins that bind RNA were just a couple of the molecular functions enriched for (enrichment over DMSO >1.5 and *P* value <0.25) by SAFs **1–16**. Among the identified proteins were GSTP1, NME1 and CRABP2, all of which have previously demonstrated reactivity towards arylfluorosulfates[4,6]. Notably, we found strong enrichment of several therapeutically important proteins that were not previously targeted by arylfluorosulfates. These included PARP1 and PARP2, critical members of DNA damage-repair pathways and validated therapeutic targets for BRCA-mutant-associated breast and ovarian cancers[16,17]. Also targeted were the macrophage migration inhibitory factor (MIF), which enhances the metastatic potential of certain cancers and acts as a pro-inflammatory signal in both chronic and acute inflammatory diseases[18,19], soluble epoxide hydrolase (EPHX2), which has garnered attention as a pharmacological target for the treatment of certain cardiovascular diseases[20], and branched chain amino acid transaminase 1 (BCAT1), which is a therapeutic target for myeloid leukaemia, carcinoma, glioblastoma and certain breast cancers[21–23]. Although we observed enrichment for 137 proteins that have been targeted by other SuFEx-derived electrophiles, more than 72% of the 491 proteins identified by SAFs **1–16** are distinct from those identified using arylfluorosulfates[4,6] or sulfonyl fluorides[24–27] (Supplementary Fig. 2c).

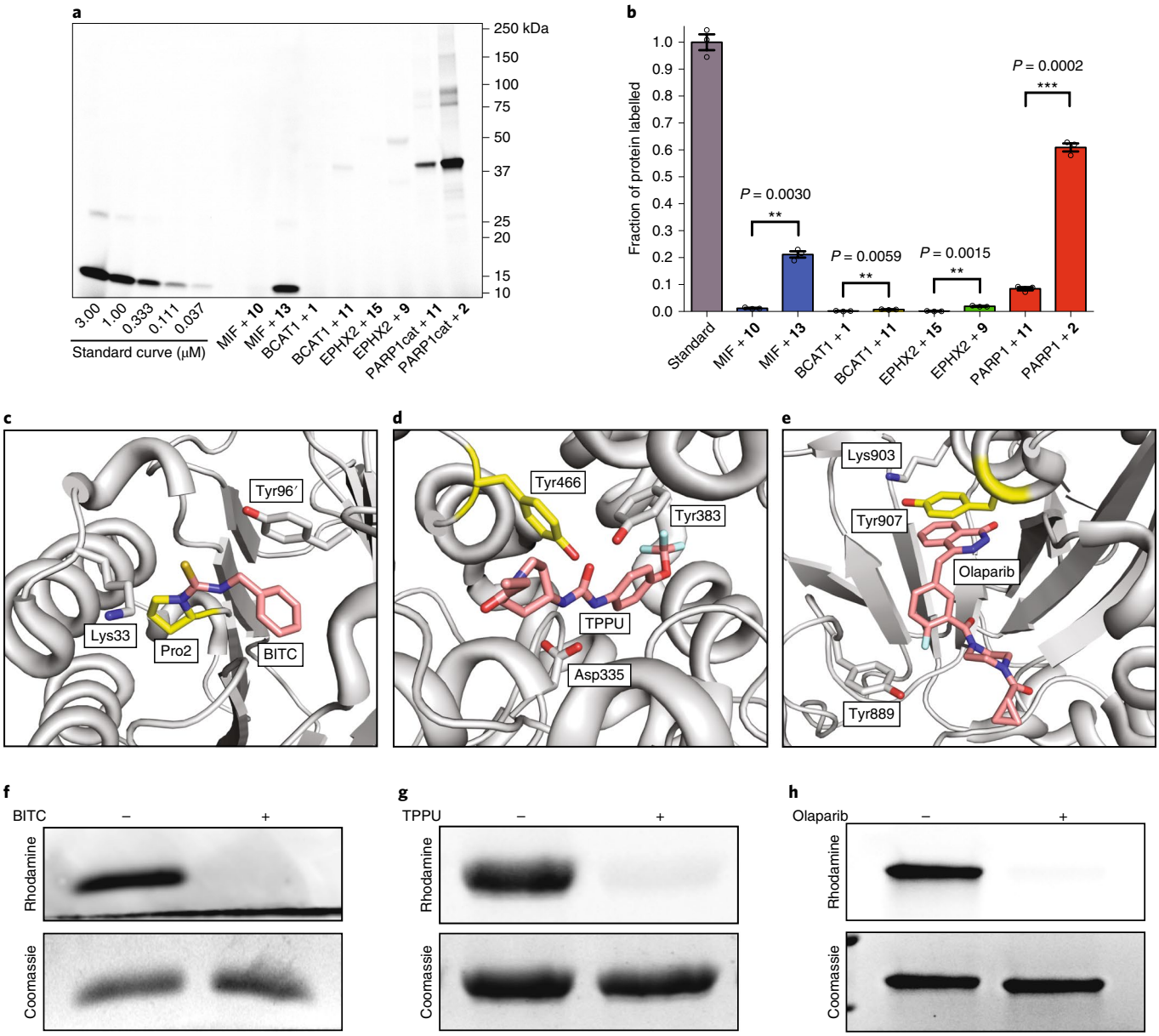

Fig. 3 | Validation of reactions between SAFs and selected recombinant proteins. a, Fluorescence-based analysis of reactions (24 h) between selected SAFs (30 μM) and selected proteins (3 μM). The standard curve comprises four threefold dilutions of fluorescently labelled MIF (3.00–0.037 μM). This gel is representative of three independent experiments ($n = 3$). **b**, Quantification of the fluorescence bands in **a**. Error bars represent ± s.e.m. for three independent experiments ($n = 3$). *P* values were calculated using a two-tailed, unpaired *t*-test. $^{**}P \leq 0.01$, $^{***}P \leq 0.001$; exact P values are shown. **c**, X-ray crystal structure of MIF conjugated to BITC, with Tyr96′ from the adjacent monomer (PDB ID 3WNT). **d**, X-ray crystal structure of EPHX2 bound to TPPU (PDB ID 4OD0). **e**, X-ray crystal structure of the PARP1cat domain bound to olaparib (PDB ID 5DS3). Residues highlighted in yellow denote the SAF-reactive nucleophiles identified by LC–MS/MS. Other labelled residues denote other potential binding sites and/or residues that may be important for reaction with the SAFs (**c**–**e**). **f**, Fluorescence-based analysis of the reaction of MIF (5 μM) and **13** (50 μM) for 24 h in the presence or absence of BITC (50 μM). This experiment was conducted once ($n = 1$). **g**, Fluorescence-based analysis of the reaction of EPHX2 (3 μM) and **9** (50 μM) for 24 h in the presence or absence of TPPU (10 μM). This experiment was conducted once ($n = 1$). **h**, Fluorescence-based analyses of the reaction of PARP1cat (3 μM) with **2** (100 μM) for 24 h in the presence or absence of olaparib (10 μM). This experiment was conducted once ($n = 1$).

Validation of selected SAF–protein reactions. To validate SAF-reactive proteins identified by affinity chromatography–MS/MS, we expressed and purified four therapeutically important proteins and reacted each purified protein with either a SAF that exhibited a high enrichment ratio (a 'positive' hit) or one that afforded a low or no enrichment (a 'negative' hit). For PARP1, we expressed only the catalytic domain (PARP1cat). Compounds **13**, **11**, **9** and **2** were selected as the positive hits for MIF, BCAT1, EPHX2 and PARP1cat, respectively, and compounds **10**, **1**, **15** and **11** were selected as negative hits for the same proteins, respectively. After a reaction period of 18 hours, each protein (3 μM) was subjected to CuAAC reactions with TMR-N_3 and the conjugates were separated by SDS–PAGE and visualized by fluorescence (Fig. 3a). In all four cases, the positive hits reacted more than the negative ones with their respective proteins, and exhibited statistical significance (Fig. 3b). It appears that neither BCAT1 nor EPHX2 were particularly reactive

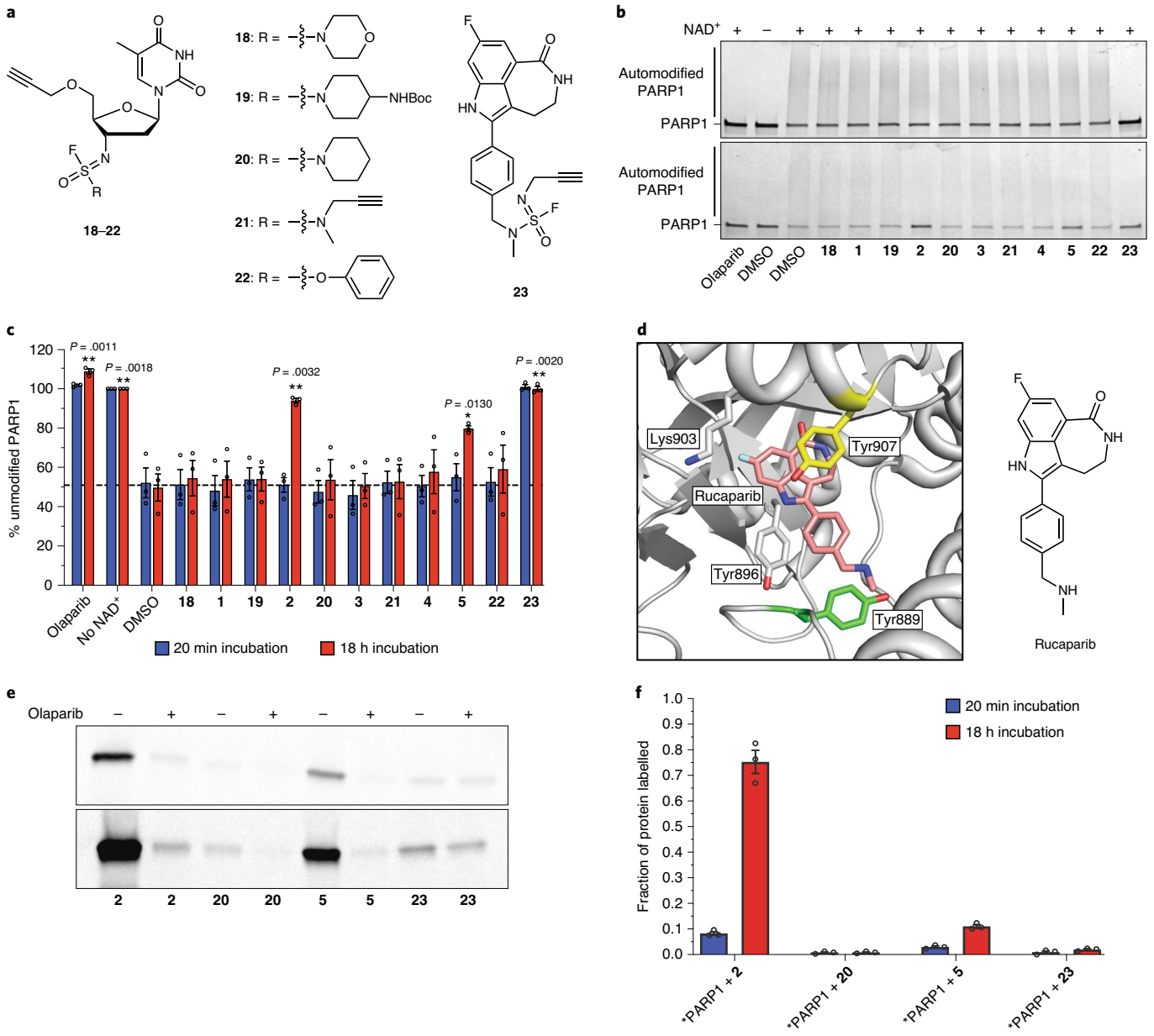

Fig. 4 | Analysis of PARP1 inhibitory activity of a subset of SAFs. a, Structures of SAFs **18**–**23** used in a PARP1 automodification assay. Left: the structures of **18**–**22**, which all share a common thymidine core structure, with the affixed 2° amine differing between them. Right: the structure of compound **23**. None of these compounds were subjected to the IDD workflow (Fig. 2a) used to identify SAF-reactive proteins. **b**, SDS–PAGE analysis of an in vitro assay of PARP1 activity. PARP1 was incubated with the indicated compound for either 20 min (top) or 18 h (bottom), and then NAD^+ (100 μM) was added. Automodification reactions were run for 1 h at room temperature before analysis. **c**, Quantification of SDS–PAGE in **b**. Error bars represent ± s.e.m. for three independent experiments ($n = 3$). *P* values were determined using a two-tailed, paired *t*-test. $^*P \leq 0.05$, $^{**}P \leq 0.01$ compared with samples treated with DMSO (see Source Data for the analysis and exact *P* values). The dashed line at 53.5% indicates the approximate baseline of unmodified PARP1 in vitro (average between vehicle treatments at 20 min and 18 h). **d**, Left: X-ray crystal structure of rucaparib bound in the NAD^+ binding site of PARP1cat (PDB ID 4RV6). Tyr907 (the SAF-reactive residue) is highlighted in yellow, and proximal Tyr889 is highlighted in green. Rucaparib is highlighted in pink. Right: the structure of the FDA-approved PARP1 inhibitor rucaparib. **e**, In-gel fluorescence analysis of reactions between PARP1cat (3 μM) and selected SAF probes (30 μM). Olaparib (30 μM) was added as a control to negate the reaction within the NAD^+ binding site of PARP1cat. PARP1cat was incubated with the indicated compound for either 20 min (top) or 18 h (bottom) before the reactions were subjected to CuAAC conditions. **f**, Quantification of in-gel fluorescence in **e**. Error bars represent ± s.e.m. for three independent experiments ($n = 3$). Results from reactions that contain olaparib are omitted for clarity.

towards their SAF probes. This may be explained by the loss of a critical post-translational modification(s) in the recombinant protein and/or different conditions experienced in lysate versus those experienced in buffer alone. Both EPHX2 and BCAT1 are known to be sensitive to the redox potential of their media[28,29], which may induce conformational changes that affect the binding and/or reactivity of the SAF. Compound **17** (not included in our library of 16 compounds), was found to react quantitatively and stoichiometrically with MIF after 16 hours at 25 °C in vitro, as determined by LC–electrospray ionization (ESI) MS (Supplementary Fig. 3).

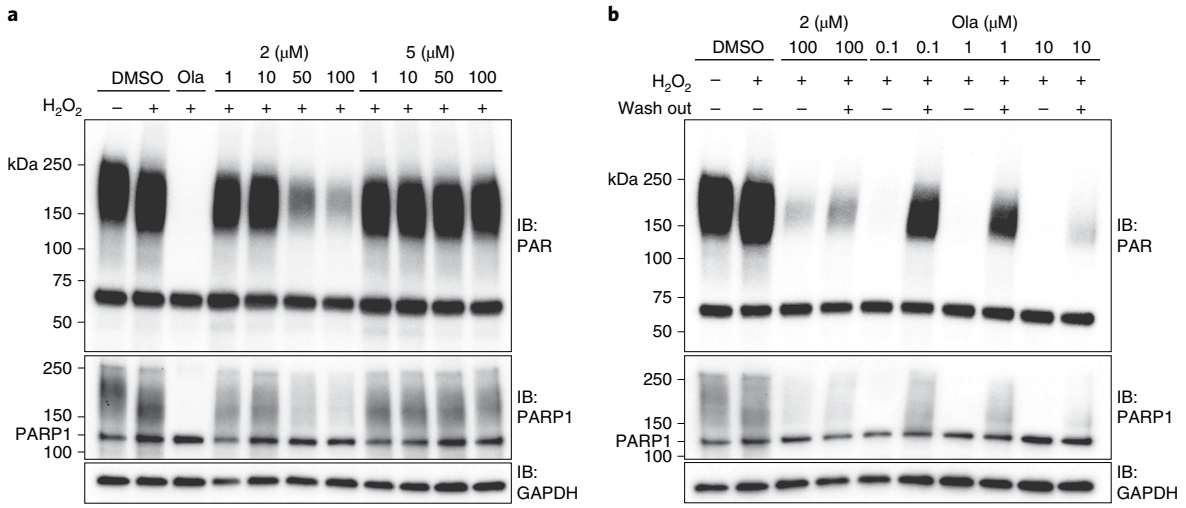

Fig. 5 | SAF 2 irreversibly inhibits the activity of PARP1 in HeLa cells. a, Immunoblot (IB) analysis of PARylation in HeLa cells treated with SAFs. The cells were incubated with olaparib (ola, positive control), **2** or **5** at increasing concentrations for 24 h before the addition of H_2O_2 (10 mM). Blots were analysed with antibodies that targeted either PAR (top) or PARP1 (middle). The reduction of both PAR and PAR-modified PARP1 (that is, a higher molecular weight smear in the middle panel) indicates the inhibition of PARP1's enzymatic activity. This experiment was conducted once ($n=1$). **b**, Western blot analysis of PARylation after HeLa cells were treated with either **2** (100 μM) or olaparib (0.1–10 μM) for 24 h and the compounds removed by washing cells twice with PBS (pH 7.4). Blots were analysed with antibodies that targeted either PAR (top) or PARP1 (middle). The reduction of both PAR and PAR-modified PARP1 in cells treated with **2** and washed indicate that **2** inhibited PARP1 irreversibly. This experiment was conducted once ($n=1$). GAPDH, glyceraldehyde 3-phosphate dehydrogenase.

Therefore, a standard curve that comprises serial dilutions from 3 μM to 37 nM in threefold decrements of recombinant MIF fully conjugated to **17** and tetramethylrhodamine was included on each denaturing gel to quantify the extent of each reaction (Fig. 3a and Supplementary Fig. 4).

SAF-reactive sites on three target proteins. To gain further insights into the SAF conjugation sites, we reacted three of the purified proteins with the SAF used to identify it from the human proteome in the presence of known active site inhibitors (Fig. 3). Conjugation was again confirmed by subjecting these in vitro reactions to a CuAAC reaction with TMR-N_3 and examining the results via SDS-PAGE. Addition of the validated MIF-reactive compound benzyl isothiocyanate (BITC; 50 μM), which forms a bond with the N-terminal proline residue (Pro1) of MIF[30] (Fig. 3c), to the reaction of recombinant MIF (5 μM) and **13** (50 μM) strongly attenuates the conjugate formation (Fig. 3f). This suggests that SAF probe **13** reacts with Pro1 or a nearby residue. This result was further confirmed by LC–MS/MS analysis of the MIF·**13** conjugate (Supplementary Fig. 5). In a similar fashion, addition of the documented EPHX2 non-covalent inhibitor 1-trifluoromethoxyphenyl-3-(1-propionylpiperidin-4-yl) urea (TPPU; 10 μM)[31] (Fig. 3d) to the reaction of recombinant EPHX2 (3 μM) with **9** (50 μM) largely ablates the fluorescence signal (Fig. 3g), which indicates that **9** occupies the enzyme's active site. This site contains two tyrosine residues, Tyr383 and Tyr466, that carry out the hydrolysis of certain lipid epoxides[29]. Either of these two catalytic residues appear to be a likely site of reaction between the SAFs and EPHX2, as both of them are susceptible to nitration[32]. Analysis of the EPHX2·**9** conjugate by LC–MS/MS implicates Tyr466 as the reactive residue in EPHX2 (Supplementary Fig. 6). Note that **9** also contains an arylfluorosulfate; however, the reaction between **9** and EPHX2 occurs at the SAF electrophilic centre, as this protein is enriched by other SAFs (**1** and **12**) that do not harbour arylfluorosulfates. To support the hypothesis that this reaction occurs at the SAF sulfur centre and not the fluorosulfate, we subjected EPHX2 to reaction with an additional compound, **9***, that shares a structural similarity with **9** but lacks a fluorosulfate. Subsequent analysis of the resulting conjugate by LC–MS/MS confirmed that the reaction between EPHX2 and **9*** takes place at Tyr466, the same residue that reacts with **9** (Supplementary Fig. 7). A labelling reaction between PARP1cat and **2** in the presence of the PARP1 non-covalent inhibitor olaparib[33] (Fig. 3e) abolished covalent conjugate formation (Fig. 3h), which indicates that **2** modifies PARP1 in the nicotinamide adenine dinucleotide (NAD^+) binding site[34]. By subjecting the reaction of **2** with PARP1cat to LC–MS/MS analysis, we determined that **2** reacts with Tyr907 in this site to form the PARP1·**2** conjugate (Supplementary Fig. 8). This was further confirmed by a strongly attenuated reaction between **2** and the Y907F mutant of PARP1cat (as compared with that of wild-type PARP1cat) (Supplementary Fig. 9). Although we cannot rule out allosteric mechanisms of competition, the previously reported ligands BITC, TPPU and olaparib appear to bind proximal to the SAF-reactive residues in MIF, EPHX2 and PARP1cat, respectively.

SAFs inhibit PARP1 activity in vitro. PARP1 executes a critical signalling post-translation modification in response to single-stranded DNA breaks. Using NAD^+, it mediates polymerization of ADP-ribose onto itself and other target proteins[35]. The newly synthesized poly(ADP-ribose) (PAR) chains act as a signal for the recruitment of diverse families of proteins to the sites of DNA damage[36]. Given the status of PARP1 as a validated pharmacological target, we sought to confirm that the reaction with SAF probes inhibits the enzyme's activity. We examined the activity of PARP1 in the presence of selected SAFs, of which all shared a common propargyl thymidine structure except **23** (Fig. 4a). Preincubation of PARP1 with activated damaged DNA and the SAF compound for 20 minutes before the addition of NAD^+ resulted in a limited inhibition of PARP1, with the notable exception of **23**, which exhibited substantial inhibition (Fig. 4b). However, notable inhibition was observed with **2** and **5** after a reaction period of 18 hours (Fig. 4b,c). Compound **23** shares considerable structural similarity with rucaparib, another Food and Drug Administration (FDA)-approved PARP1 inhibitor[37,38]. Examination of the co-crystal structure of PARP1cat bound to rucaparib (Fig. 4d, Protein Data Bank (PDB)

ID 4RV6), led us to posit that the inhibitory effects of **23** are mediated primarily through non-covalent interactions with PARP1, in contrast with the considerable conjugation demonstrated by **2** and **5**. To test this hypothesis, we subjected **2**, **5**, **20** and **23** to reactions with PARP1cat for 20 minutes or 18 hours, followed by a CuAAC reaction with TMR-N_3. The results were quantified by fluorescent SDS-PAGE (Fig. 4e,f). It is clear that **23** did not react with PARP1cat above background. We hypothesize that **23** adopts a binding orientation close to that of rucaparib in the NAD^+-binding site of PARP1cat, which prevents the SAF from engaging with Tyr907. However, SAFs **2** and **5** react substantially with PARP1cat, with some reaction occurring after just 20 minutes at 25 °C. These results suggest that to simply modify the existing structures of known protein ligands with SAF electrophiles does not generally result in a conjugation reaction, which emphasizes the importance of a proper positioning of the SAF.

SAF 2 inhibits PAR synthesis in HeLa cells. To investigate whether SAFs inhibit PARP1 activity in living cells, we treated HeLa cells with **2**, **5** or olaparib for 24 hours prior to the addition of H_2O_2 for 15 minutes to induce PARylation. No cell death was observed over this period. After cell lysis, the extent of the PAR modification was measured by immunoblot using antibodies that recognize PAR and PARP1. Cells treated with **2** exhibited a substantial reduction in both general PARylation and PARP1 automodification, unlike cells treated with **5** or vehicle alone (Fig. 5a). As expected, treatment with olaparib (positive control) resulted in the total ablation of PAR synthesis. The ability of **2** to inhibit PARP1 activity in cells is notable, given that its structure has not been optimized for cellular permeability nor PARP1 binding by medicinal chemistry efforts.

To scrutinize the cellular activity, we subjected HeLa cells to a treatment with either olaparib or **2** for 24 hours. Cells were then washed and fresh media (free of inhibitor) was added for 6 hours. PARP1 activity was then induced via treatment with H_2O_2. This treatment regimen by **2** retained most of its PARP1 inhibitory activity, whereas the olaparib activity was dramatically reduced (Fig. 5b), which indicates that conjugation by **2** inhibits PAR synthesis until the enzyme is turned over.

Discussion

Past drug-discovery efforts, by and large, have not deliberately leveraged functional groups capable of protein conjugation. This may be due to concerns about off-target reactivity and associated toxicity. However, the recent emergence of new functional groups that exhibit highly attenuated or latent protein reactivity, such as those capable of undergoing a SuFEx reaction, suggest that drug discovery efforts that make deliberate use of these functionalities could produce highly selective covalent drugs[2,6,26]. Our previous IDD approach with arylfluorosulfates led to validated covalent probes for 11 human proteins[4]. In this study, a new set of proteins closely associated with pathology (for example, BCAT1, EPHX2, PARP1 and MIF) were matched with SAFs via the IDD strategy. Recombinant BCAT1 and EPHX2 exhibited a low reactivity towards their corresponding SAF probes, which suggests that extensive medicinal chemistry would be required to modulate function with SAFs. Conversely, MIF and PARP1 exhibited a robust reactivity towards SAFs from our first-generation library, which suggests that the discovery of more reactive and selective SAF compounds towards these proteins would probably require less effort. Notably, we demonstrated that **2** inhibited PARP1 function in living cancer cells even after compound washout, which implies that the SAF-based inhibition of PARP1 may represent a viable anticancer strategy.

Acquired or inherited defects in the DNA system for damage response and repair increase the lifetime risk of cancer. Mutations in BRCA1 and BRCA2, both DNA repair proteins, were some of the first mutations to be associated with familial breast and ovarian cancers[39,40]. The targeting of PARP1 is appealing because of the 1980 demonstration that the inhibition of PARP1 sensitized leukaemia cells to cytotoxic alkylating agents[41]. This premise was built on by an abundance of preclinical evidence that supports the ability of PARP inhibitors to sensitize and potentiate radiation and cytotoxic chemotherapy[42]. However, the pivotal breakthrough was made with the observation that BRCA-mutant cells were up to 1,000 times more sensitive to PARP inhibitors[43,44]. The enhanced sensitivity observed in BRCA-mutant cancer cells enabled the clinical validation of synthetic lethality in oncology, a concept first described in 1922, wherein simultaneous targeting of two genes or proteins can be lethal, even when deletion and/or inhibition of each individually is itself tolerated[45,46].

The treatment of cancers with existing PARP1 inhibitors is associated with a high incidence of toxicity (such as neutropenia and anaemia)[47]. New PARP1 inhibitors based on a covalent mechanism of action may allow for the circumvention of side effects associated with existing inhibitors. It was recently reported that PAR synthesis helps drive α-synuclein aggregation both in vitro and in vivo, which highlights PARP1 inhibition as a potential therapy for the treatment of Parkinson's disease[48]. Such a therapy will most probably require an extended duration of action, a convenient feature of SAF-based PARP1 inhibitors[49]. It is notable that our PARP1-reactive compounds bear little structural resemblance to the FDA-approved inhibitors (for example, olaparib). Our compounds represent a fresh start for inhibitor design and synthesis. Covalent PARP1 inhibitors may be optimized to achieve selective PARP1 or PARP2 inhibition, whereas non-covalent inhibitors are expected to bind to a wider array of PARP family members[38].

The apparent low reactivity of SAFs means that only a subset of the human proteome is even capable of reacting with this functional group, which substantially reduces the off-target reactivity observed with more-reactive electrophiles. This feature, combined with their chirality and straightforward synthesis, makes SAFs ideally suited for the rapid generation of compound libraries, and so potentially simplify the optimization of identified hits based on medicinal chemistry. For IDD that involves arylfluorosulfates, the electrophilic warhead and affinity handle must be installed at separate sites via separate reactions or the judicious use of one-pot reaction schemes. As a result, the applicability of the arylfluorosulfates in library construction is more challenging. For these reasons, we recommend that future IDD efforts take seriously the potential of SAFs.

Online content

Any methods, additional references, Nature Research reporting summaries, source data, extended data, supplementary information, acknowledgements, peer review information; details of author contributions and competing interests; and statements of data and code availability are available at https://doi.org/10.1038/s41557-020-0530-4.

Received: 25 April 2019; Accepted: 23 July 2020;
Published online: 31 August 2020

References

1. Macarron, R. et al. Impact of high-throughput screening in biomedical research. *Nat. Rev. Drug Disc.* **10**, 188–195 (2011).
2. Singh, J., Petter, R. C., Baillie, T. A. & Whitty, A. The resurgence of covalent drugs. *Nat. Rev. Drug Disc.* **10**, 307–317 (2011).
3. Bauer, R. A. Covalent inhibitors in drug discovery: from accidental discoveries to avoided liabilities and designed therapies. *Drug Disc. Today* **20**, 1061–1073 (2015).
4. Mortenson, D. E. et al. 'Inverse drug discovery' strategy to identify proteins that are targeted by latent electrophiles as exemplified by aryl fluorosulfates. *J. Am. Chem. Soc.* **140**, 200–210 (2018).
5. Dong, J., Krasnova, L., Finn, M. G. & Sharpless, K. B. Sulfur(VI) fluoride exchange (SuFEx): another good reaction for click chemistry. *Angew. Chem. Int. Ed.* **53**, 9430–9448 (2014).
6. Chen, W. et al. Arylfluorosulfates inactivate intracellular lipid binding protein(s) through chemoselective SuFEx reaction with a binding site Tyr residue. *J. Am. Chem. Soc.* **138**, 7353–7364 (2016).

7. Dong, J., Sharpless, K. B., Kwisnek, L., Oakdale, J. S. & Fokin, V. V. SuFEx-based synthesis of polysulfates. *Angew. Chem. Int. Ed.* **53**, 9466–9470 (2014).
8. Gao, B. et al. Bifluoride-catalysed sulfur(vi) fluoride exchange reaction for the synthesis of polysulfates and polysulfonates. *Nat. Chem.* **9**, 1083–1088 (2017).
9. Wang, H. et al. SuFEx-based polysulfonate formation from ethenesulfonyl fluoride–amine adducts. *Angew. Chem. Int. Ed.* **56**, 11203–11208 (2017).
10. Liu, Z. et al. SuFEx click chemistry enabled late-stage drug functionalization. *J. Am. Chem. Soc.* **140**, 2919–2925 (2018).
11. Li, S., Wu, P., Moses, J. E. & Sharpless, K. B. Multidimensional SuFEx click chemistry: sequential sulfur(vi) fluoride exchange connections of diverse modules launched from an SOF_4 hub. *Angew. Chem. Int. Ed.* **56**, 2903–2908 (2017).
12. Wang, Q. et al. Bioconjugation by copper(i)-catalyzed azide–alkyne [3+2] cycloaddition. *J. Am. Chem. Soc.* **125**, 3192–3193 (2003).
13. Rostovtsev, V. V., Green, L. G., Fokin, V. V. & Sharpless, K. B. A stepwise Huisgen cycloaddition process: copper(i)-catalyzed regioselective 'ligation' of azides and terminal alkynes. *Angew. Chem. Int. Ed.* **41**, 2596–2599 (2002).
14. Verhelst, S. H., Fonovic, M. & Bogyo, M. A mild chemically cleavable linker system for functional proteomic applications. *Angew. Chem. Int. Ed.* **46**, 1284–1286 (2007).
15. Dayon, L. et al. Relative quantification of proteins in human cerebrospinal fluids by MS/MS using 6-plex isobaric tags. *Anal. Chem.* **80**, 2921–2931 (2008).
16. Konecny, G. E. & Kristeleit, R. S. PARP inhibitors for BRCA1/2-mutated and sporadic ovarian cancer: current practice and future directions. *Br J. Cancer* **115**, 1157–1173 (2016).
17. Lord, C. J. & Ashworth, A. BRCAness revisited. *Nat. Rev. Cancer* **16**, 110–120 (2016).
18. Lue, H., Kleemann, R., Calandra, T., Roger, T. & Bernhagen, J. Macrophage migration inhibitory factor (MIF): mechanisms of action and role in disease. *Microbes Infect.* **4**, 449–460 (2002).
19. Calandra, T. & Roger, T. Macrophage migration inhibitory factor: a regulator of innate immunity. *Nat. Rev. Immunol.* **3**, 791–800 (2003).
20. Imig, J. D. & Hammock, B. D. Soluble epoxide hydrolase as a therapeutic target for cardiovascular diseases. *Nat. Rev. Drug Disc.* **8**, 794–805 (2009).
21. Tonjes, M. et al. BCAT1 promotes cell proliferation through amino acid catabolism in gliomas carrying wild-type IDH1. *Nat. Med.* **19**, 901–908 (2013).
22. Xu, M. et al. BCAT1 promotes tumor cell migration and invasion in hepatocellular carcinoma. *Oncol. Lett.* **12**, 2648–2656 (2016).
23. Zhang, L. & Han, J. Branched-chain amino acid transaminase 1 (BCAT1) promotes the growth of breast cancer cells through improving mTOR-mediated mitochondrial biogenesis and function. *Biochem. Biophys. Res. Commun.* **486**, 224–231 (2017).
24. Zhao, Q. et al. Broad-spectrum kinase profiling in live cells with lysine-targeted sulfonyl fluoride probes. *J. Am. Chem. Soc.* **139**, 680–685 (2017).
25. Zheng, Q. et al. SuFEx-enabled, agnostic discovery of covalent inhibitors of human neutrophil elastase. *Proc. Natl Acad. Sci. USA* **116**, 18808–18814 (2019).
26. Hett, E. C. et al. Rational targeting of active-site tyrosine residues using sulfonyl fluoride probes. *ACS Chem. Biol.* **10**, 1094–1098 (2015).
27. Hanoulle, X. et al. A new functional, chemical proteomics technology to identify purine nucleotide binding sites in complex proteomes. *J. Proteome Res.* **5**, 3438–3445 (2006).
28. Goto, M. et al. Structural determinants for branched-chain aminotransferase isozyme-specific inhibition by the anticonvulsant drug gabapentin. *J. Biol. Chem.* **280**, 37246–37256 (2005).
29. Morisseau, C. & Hammock, B. D. Epoxide hydrolases: mechanisms, inhibitor designs, and biological roles. *Ann. Rev. Pharmacol. Toxicol.* **45**, 311–333 (2005).
30. Spencer, E. S. et al. Multiple binding modes of isothiocyanates that inhibit macrophage migration inhibitory factor. *Eur. J. Med. Chem.* **93**, 501–510 (2015).
31. Lee, K. S. et al. Optimized inhibitors of soluble epoxide hydrolase improve in vitro target residence time and in vivo efficacy. *J. Med. Chem.* **57**, 7016–7030 (2014).
32. Barbosa-Sicard, E. et al. Inhibition of the soluble epoxide hydrolase by tyrosine nitration. *J. Biol. Chem.* **284**, 28156–28163 (2009).
33. Fong, P. C. et al. Inhibition of poly(ADP-ribose) polymerase in tumors from BRCA mutation carriers. *N. Engl. J. Med.* **361**, 123–134 (2009).
34. Dawicki-McKenna, J. M. et al. PARP-1 activation requires local unfolding of an autoinhibitory domain. *Mol. Cell* **60**, 755–768 (2015).
35. Langelier, M.-F., Servent, K. M., Rogers, E. E. & Pascal, J. M. A third zinc-binding domain of human poly(ADP-ribose) polymerase-1 coordinates DNA-dependent enzyme activation. *J. Biol. Chem.* **283**, 4105–4114 (2008).
36. Gibson, B. A. & Kraus, W. L. New insights into the molecular and cellular functions of poly(ADP-ribose) and PARPs. *Nat. Rev. Mol. Cell Biol.* **13**, 411–424 (2012).
37. Coleman, R. L. et al. Rucaparib maintenance treatment for recurrent ovarian carcinoma after response to platinum therapy (ARIEL3): a randomised, double-blind, placebo-controlled, phase 3 trial. *The Lancet* **390**, 1949–1961 (2017).
38. Thorsell, A.-G. et al. Structural basis for potency and promiscuity in poly(ADP-ribose) polymerase (PARP) and tankyrase inhibitors. *J. Med. Chem.* **60**, 1262–1271 (2017).
39. Futreal, P. et al. BRCA1 mutations in primary breast and ovarian carcinomas. *Science* **266**, 120–122 (1994).
40. Wooster, R. et al. Identification of the breast cancer susceptibility gene BRCA2. *Nature* **378**, 789–792 (1995).
41. Durkacz, B. W., Omidiji, O., Gray, D. A. & Shall, S. (ADP-ribose)n participates in DNA excision repair. *Nature* **283**, 593–596 (1980).
42. Tentori, L. & Graziani, G. Chemopotentiation by PARP inhibitors in cancer therapy. *Pharmacol. Res.* **52**, 25–33 (2005).
43. Bryant, H. E. et al. Specific killing of BRCA2-deficient tumours with inhibitors of poly(ADP-ribose) polymerase. *Nature* **434**, 913–917 (2005).
44. Farmer, H. et al. Targeting the DNA repair defect in BRCA mutant cells as a therapeutic strategy. *Nature* **434**, 917–921 (2005).
45. Nijman, S. M. B. Synthetic lethality: general principles, utility and detection using genetic screens in human cells. *FEBS Lett.* **585**, 1–6 (2011).
46. Bridges, C. B. The origin of variations in sexual and sex-limited characters. *Am. Nat.* **56**, 51–63 (1922).
47. Pujade-Lauraine, E. et al. Olaparib tablets as maintenance therapy in patients with platinum-sensitive, relapsed ovarian cancer and a BRCA1/2 mutation (SOLO2/ENGOT-Ov21): a double-blind, randomised, placebo-controlled, phase 3 trial. *Lancet Oncol.* **18**, 1274–1284 (2017).
48. Kam, T.-I. et al. Poly(ADP-ribose) drives pathologic α-synuclein neurodegeneration in Parkinson's disease. *Science* **362**, eaat8407 (2018).
49. Berger, N. A. et al. Opportunities for the repurposing of PARP inhibitors for the therapy of non-oncological diseases. *Br. J. Pharmacol.* **175**, 192–222 (2018).

Methods

Proteome labelling, fluorescence SDS–PAGE and SAF–protein conjugate affinity purification. Conjugation reactions were carried out as follows: 5 µl of either DMSO or a 10 mM solution of the SAF compound in DMSO were added to 995 µl of HEK293T lysate, followed by incubation at 25 °C for 18 h. After the proteome reaction period, 50 µl of each reaction was subjected to CuAAC reaction conditions with TMR-N_3 (ThermoFisher Scientific). The CuAAC conditions were: 2 µl of 20 µM $CuSO_4$, 2 µl of 40 mM BTTAA (Click Chemistry Tools), 2.5 µl of sodium ascorbate (Sigma-Aldrich) and 1 µl of 5 mM TMR-N_3 (in DMSO) were added to 50 µl of each proteome labelling reaction, and the reactions were incubated at 30 °C for 1 h. Afterwards, proteins in the reaction mixture were precipitated by the addition of MeOH/$CHCl_3$ (3:1). The proteins were resuspended and subsequently pelleted twice in MeOH to facilitate the removal of excess TMR-N_3. After the final removal of MeOH by aspiration, the proteins were dissolved in reducing SDS loading buffer. Proteins were resolved by SDS–PAGE, and the fluorescently labelled proteins were visualized using a ChemiDoc XRS+ imager (Bio-Rad). Gels were then stained with a NOVEX Colloidal Blue Stain Kit (Invitrogen) to assess equal protein loading across all lanes.

Protein–SAF conjugates were purified, digested and TMT mass tagged in accordance with a published experimental procedure[4]. Briefly, 950 µl of each proteome conjugation reaction described above were subjected to CuAAC reaction conditions, with TMR-N_3 substituted by diazo biotin-N_3 (Click Chemistry Tools, catalogue no. 1041). The reaction conditions were: 20 µl of 20 µM $CuSO_4$, 20 µl of 40 mM BTTAA, 50 µl of sodium ascorbate and 10 µl of 5 mM biotin-N_3 (DMSO) were added to 950 µl of each proteome labelling reaction, and the reactions were incubated at 30 °C for 2 h. After the CuAAC reaction, the proteins subjected to the conjugation reaction were precipitated by the addition of MeOH/$CHCl_3$ (3:1) and subsequently pelleted by centrifugation. The supernatant was removed by aspiration, and the pellet was washed with MeOH three times to remove excess biotin-N_3. After briefly drying the pellets in air following the removal of MeOH, proteome samples were resuspended in a 6 M urea solution that contained 25 mM $(NH_4)HCO_3$. SDS (as a 10% solution w/v in water) was added to a final concentration of 2.2% to solubilize the protein pellets. Next, proteins were reduced by the addition of 1 M dithiothreitol to a final concentration of 7.8 mM and incubation for 15 min at 65 °C. After cooling briefly on ice, the proteins were alkylated by the addition of 0.5 M iodoacetamide (Sigma-Aldrich) to a final concentration of 29 mM and incubated in the dark for 30 min at 25 °C. Proteome samples were each diluted into 6 ml of PBS that contained High-Capacity Streptavidin Agarose Resin (ThermoFisher Scientific) and allowed to incubate for 16 h with gentle agitation. The resin was then washed: once with PBS + 1% SDS, and then twice with PBS that contained no detergent. The labelled proteins were then eluted from the resin by incubating for 1 h at 25 °C with PBS that contained 1% SDS and 50 mM $Na_2S_2O_4$ (the solution was quickly adjusted to pH ~7 after the dissolution of $Na_2S_2O_4$). The elution procedure was carried out twice and the elution volumes combined. The subsequently enriched proteins were then precipitated once again with MeOH/$CHCl_3$ (3:1), the pellets were washed and centrifuged twice with MeOH to remove traces of SDS and were then dried in air to remove residual MeOH. The proteins were then resuspended in a solution that contained 0.2% Rapigest detergent (Waters) and 100 mM HEPES pH 8.0, and were digested overnight with trypsin protease (mass-spectrometric grade; ThermoFisher Scientific). The digested samples were then reacted with their designated TMT 6-plex reagent (ThermoFisher Scientific) for 1 h (reactions were conducted in 40% acetonitrile), and the reactions were quenched by the addition of 10% $(NH_4)HCO_3$ (w/v) for 1 h to a final concentration of 0.4% (w/v). The quenched reactions were then combined and acidified to pH < 2 by the addition of formic acid. The acetonitrile used in the TMT-labelling reaction was removed via centrifugation under reduced pressure, and the samples were incubated at 42 °C for 1 h to precipitate the remaining Rapigest. The samples were then centrifuged and the supernatants collected and loaded into columns for multidimensional protein identification technology experiments, as previously described[50]. A heatmap was generated with R (version 3.2.4) using enrichment ratios for hand-selected proteins identified by the multidimensional protein identification technology experiments.

Fluorescence-based analysis of reactions between selected SAFs and selected proteins. Reactions were carried out at room temperature in PBS (pH 7.4). Protein (MIF, BCAT1, EPHX2 or PARP1cat; 3 µM) were incubated with 30 µM of the indicated SAF compound for 24 h at room temperature. Aliquots (50 µl) of each reaction were subjected to CuAAC reaction conditions with TMR-N_3 (described above). The reactions were then treated with 12 µl of 6× SDS loading buffer, followed by SDS–PAGE. The fluorescently labelled protein was visualized using a ChemiDoc XRS+ imager (Bio-Rad). Fluorescent bands were quantified using Image Lab (BioRad) and plotted using Prism 6 (GraphPad). Error bars represent ± s.e.m. for three independent experiments. Statistical significance was calculated with the unpaired Student's *t*-test: $^{**}P \leq 0.01$, $^{***}P \leq 0.001$. The extent of the SAF–protein reactions was quantified using a fluorescent MIF standard curve. MIF (10 µM) in PBS was reacted with **17** (100 µM) for 24 h at room temperature (~25 °C), after which time reaction completion was confirmed via LC–MS analysis using a 1260 Infinity LC System (Agilent Technologies) and a 6130 Quadrupole LC/MS (Agilent Technologies). Protein *m/z* was calculated using the Deconvolution Tool in the OpenLab Software Sutie (Agilent Technologies). MIF was diluted to 3 µM in PBS and subjected to CuAAC reaction conditions with TMR-N_3 (described above). This solution was then diluted threefold five times into PBS that contained SDS loading buffer to make the standard curve.

Fluorescence-based analysis of the reaction between MIF and 13 (with or without BITC). MIF (5 µM) in PBS was treated with **13** (50 µM) along with either 50 µM BITC or an equivalent volume of DMSO. The reactions were carried out at room temperature for 24 h. After this time, 50 µl of each reaction was subjected to CuAAC conditions with TMR-N_3 and subsequently treated with 12 µl of 6× SDS loading buffer, followed by SDS–PAGE. The fluorescently labelled protein was then visualized using a ChemiDoc XRS+ imager (Bio-Rad). The gels were then stained with a NOVEX Colloidal Blue Stain Kit (Invitrogen) and imaged using a ChemiDoc XRS+ imager (Bio-Rad).

Fluorescence-based analysis of the reaction between EPHX2 and 9 (with or without TPPU). EPHX2 (3 µM) in PBS was treated with **9** (50 µM) along with either 10 µM TPPU or an equivalent volume of DMSO. The reactions were carried out at room temperature for 24 h. After this time, 50 µl of each reaction was subjected to CuAAC conditions with TMR-N_3 and subsequently treated with 12 µl of 6× SDS loading buffer, followed by SDS–PAGE. The fluorescently labelled protein was then visualized using a ChemiDoc XRS+ imager (Bio-Rad). The gels were then stained with a NOVEX Colloidal Blue Stain Kit (Invitrogen) and imaged using a ChemiDoc XRS+ imager (Bio-Rad).

Fluorescence-based analysis of the reaction between PARP1cat and 2 (with or without olaparib). PARP1cat (3 µM) in PBS was treated with **2** (100 µM) along with either 10 µM olaparib or an equivalent volume of DMSO. The reactions were carried out at room temperature for 24 h. After this time, 50 µl of each reaction was subjected to CuAAC conditions with TMR-N_3 and subsequently treated with 12 µl of 6× SDS loading buffer, followed by SDS–PAGE. The fluorescently labelled protein was then visualized using a ChemiDoc XRS+ imager (Bio-Rad). The gels were then stained with a NOVEX Colloidal Blue Stain Kit (Invitrogen) and imaged using a ChemiDoc XRS+ imager (Bio-Rad).

Reporting Summary. Further information on research design is available in the Nature Research Reporting Summary linked to this article.

Data availability

Additional methods and data are provided in the Supplementary Information. All data generated or analysed during this study are included in this published article (and its supplementary files). Source data are provided with this paper.

References

50. Ryno, L. M. et al. Characterizing the altered cellular proteome induced by the stress-independent activation of heat shock factor 1. *ACS Chem. Biol.* **9**, 1273–1283 (2014).

Acknowledgements

This work was supported by the Skaggs Institute for Chemical Biology, the Lita Annenberg Hazen Foundation and National Institutes of Health grants DK046335 (J.W.K.). R.C.B. was supported by a grant from the American Cancer Society. D.E.M. was supported by a grant from the George E. Hewitt Foundation for Medical Research. This work was supported in part by the National Institute of Environmental Health Sciences (NIEHS) Grant R35 ES030443, and NIEHS Superfund Research Program P42 ES004699.

Author contributions

G.J.B., R.C.B. and J.W.K. conceived and designed the experiments G.J.B., R.C.B., S.L., L.N., D.E.M., G.L., C.M. and H.W. carried out the experiments and performed the data analysis G.J.B., R.C.B., S.L., C.M., B.D.H., K.B.S. and J.W.K. co-wrote the paper.

Competing interests

The authors declare no competing interests.

Additional information

Supplementary information is available for this paper at https://doi.org/10.1038/s41557-020-0530-4.

Correspondence and requests for materials should be addressed to K.B.S. or J.W.K.

Reprints and permissions information is available at www.nature.com/reprints.

nature research

Corresponding author(s): Jeffery W. Kelly

Last updated by author(s): Apr 2, 2020

Reporting Summary

Nature Research wishes to improve the reproducibility of the work that we publish. This form provides structure for consistency and transparency in reporting. For further information on Nature Research policies, see Authors & Referees and the Editorial Policy Checklist.

Statistics

For all statistical analyses, confirm that the following items are present in the figure legend, table legend, main text, or Methods section.

n/a	Confirmed
☐	☒ The exact sample size (*n*) for each experimental group/condition, given as a discrete number and unit of measurement
☐	☒ A statement on whether measurements were taken from distinct samples or whether the same sample was measured repeatedly
☐	☒ The statistical test(s) used AND whether they are one- or two-sided *Only common tests should be described solely by name; describe more complex techniques in the Methods section.*
☒	☐ A description of all covariates tested
☒	☐ A description of any assumptions or corrections, such as tests of normality and adjustment for multiple comparisons
☒	☐ A full description of the statistical parameters including central tendency (e.g. means) or other basic estimates (e.g. regression coefficient) AND variation (e.g. standard deviation) or associated estimates of uncertainty (e.g. confidence intervals)
☐	☒ For null hypothesis testing, the test statistic (e.g. *F*, *t*, *r*) with confidence intervals, effect sizes, degrees of freedom and *P* value noted *Give P values as exact values whenever suitable.*
☒	☐ For Bayesian analysis, information on the choice of priors and Markov chain Monte Carlo settings
☒	☐ For hierarchical and complex designs, identification of the appropriate level for tests and full reporting of outcomes
☒	☐ Estimates of effect sizes (e.g. Cohen's *d*, Pearson's *r*), indicating how they were calculated

Our web collection on statistics for biologists contains articles on many of the points above.

Software and code

Policy information about availability of computer code

Data collection	Xcalibur Data Acquisition and Interpretation Software (Thermo Fisher Scientific) was used to collect MS1 and MS2 spectra from the Q Exactive Hybrid Quadrupole-Orbitrap Mass Spectrometer. Image Lab (version 6.0) was used to visualize fluorescence or coomassie stained electrophoresis gels.
Data analysis	Tandem mass spectra were extracted into MS1 and MS2 files from raw files using RawExtract 1.9.9. Protein identification and quantification analysis were conducted with Integrated Proteomics Pipeline (IP2 ver. 6.5.5, Integrated Proteomics Applications, Inc. San Diego, CA. (http://www.integratedproteomics.com) using ProLuCID/Sequest, DTASelect (version 2), and Census. Enrichment ratios and statistics were conducted using Microsoft Excel (version 16), and heatmap was generated using RStudio (version 3.2.4). Image Lab (version 6.0) was used to quantify band/lane fluorescence intensities of electrophoresis gels. Plots were generated using Microsoft Excel (version 16) and Prism 6 (Graphpad)

For manuscripts utilizing custom algorithms or software that are central to the research but not yet described in published literature, software must be made available to editors/reviewers. We strongly encourage code deposition in a community repository (e.g. GitHub). See the Nature Research guidelines for submitting code & software for further information.

Data

Policy information about availability of data

All manuscripts must include a data availability statement. This statement should provide the following information, where applicable:

- Accession codes, unique identifiers, or web links for publicly available datasets
- A list of figures that have associated raw data
- A description of any restrictions on data availability

All data generated and analyzed during this study are included in this published article (and its supplementary information)

Field-specific reporting

Please select the one below that is the best fit for your research. If you are not sure, read the appropriate sections before making your selection.

☒ Life sciences ☐ Behavioural & social sciences ☐ Ecological, evolutionary & environmental sciences

For a reference copy of the document with all sections, see nature.com/documents/nr-reporting-summary-flat.pdf

Life sciences study design

All studies must disclose on these points even when the disclosure is negative.

Sample size	Sample sizes were chosen to guarantee the reproducibility of the techniques used in the study. The techniques have low variability, therefore 2 - 3 replicates were considered sufficient.
Data exclusions	No data was excluded from this study.
Replication	Quantitative proteomics experiments (e.g. MS/MS) were conducted as duplicates of each treatment condition (e.g. with SAF X or DMSO). Reactions between recombinant proteins and SAF compounds were conducted three times in all cases. All attempts at replication were successful.
Randomization	Formal randomization was not relevant for this study. The techniques used to identify the targets of each compound are inherently unbiased towards a specific protein(s) or family of proteins.
Blinding	Formal blinding was not relevant for this study. The techniques used to identify the targets of each compound are inherently unbiased towards a specific protein(s) or family of proteins.

Reporting for specific materials, systems and methods

We require information from authors about some types of materials, experimental systems and methods used in many studies. Here, indicate whether each material, system or method listed is relevant to your study. If you are not sure if a list item applies to your research, read the appropriate section before selecting a response.

Materials & experimental systems

n/a	Involved in the study
☐	☒ Antibodies
☐	☒ Eukaryotic cell lines
☒	☐ Palaeontology
☒	☐ Animals and other organisms
☒	☐ Human research participants
☒	☐ Clinical data

Methods

n/a	Involved in the study
☒	☐ ChIP-seq
☒	☐ Flow cytometry
☒	☐ MRI-based neuroimaging

Antibodies

Antibodies used	Antibodies for PARP1 (Cell Signaling, 9542), PAR (Trevigen, 4336-BPC-100), and GAPDH (Cell Signaling, 2118) were detected with an anti-rabbit IgG HRP-linked antibody (Cell Signaling, 7074).
Validation	For the PARP1 antibody (Cell Signaling, 9542), the supplier (Cell Signaling) validated it via western blot under three different conditions, including PARP1 knock-out conditions. Use of this antibody has been cited 1988 times, according to CiteAb. For the GAPDH antibody (Cell Signaling, 2118), the supplier (Cell Signaling) validated it using western blot, immunohistochemical staining, immunofluorescent staining, and flow cytometry. Use of this antibody has been cited 2988 times, according to CiteAb. For the PAR antibody (Trevigen, 4336-BPC-100), the supplier (Trevigen) recommended applications are for Western and dot blotting. Use of this antibody has been cited at least 15 times, according to the supplier. According to CiteAb, its use has been cited 3 times.

Eukaryotic cell lines

Policy information about cell lines

Cell line source(s)	Both HEK293T cells (ATCC® CRL-3216™, Lot# 62296864) and HeLa cells (ATCC® CCL-2™, Lot# 58930571) were purchased from ATCC.

Authentication	None of the cell lines used in this study were authenticated by the authors
Mycoplasma contamination	Cell lines were not tested for mycoplasma contamination
Commonly misidentified lines (See ICLAC register)	No commonly misidentified cell lines were used.